

Ligand Migration in Human Myoglobin: Steric Effects of Isoleucine 107(G8) on O₂ and CO Binding

Haruto Ishikawa, Takeshi Uchida, Satoshi Takahashi, Koichiro Ishimori, and Isao Morishima

Department of Molecular Engineering, Graduate School of Engineering, Kyoto University, Kyoto 606-8501, Japan

ABSTRACT To investigate the ligand pathway in myoglobin, some mutant myoglobins, in which one of the amino acid residues constituting a putative ligand-docking site, Ile107, is replaced by Ala, Val, Leu, or Phe, were prepared and their structural and ligand binding properties were characterized. The kinetic barrier for the ligand entry to protein inside was lowered by decreasing the side-chain volume at position 107, indicating that the bulky side chain interferes with the formation of the activation state for the ligand migration and the free space near position 107 would be filled with the ligand in the activation state. Another prominent effect of the reduced side-chain volume at position 107 is to stabilize the ligand-binding intermediate state. Because the stabilization can be ascribed to decrease of the positive enthalpy, the enlarged free space near position 107 would relieve unfavorable steric interactions between the ligand and nearby amino acid residues. The side-chain volume at position 107, therefore, is crucial for the kinetic barrier for the ligand migration and free energy of the ligand-binding intermediate state, which allows us to propose that some photodissociated O₂ moves toward position 107 to be trapped and then expelled to the solvent.

INTRODUCTION

For more than 20 years, the pathways for ligand migration from the heme iron to solvent in myoglobin have intensively been studied, because understanding of the ligand migration in myoglobin has been considered one of the fundamental steps for the dynamics of ligand binding in hemoprotein. In most of hemoproteins, the ligand-binding reaction consists of at least two well-separated kinetic processes. One is the slower phase called the bimolecular process, and the other is the faster phase called the geminate process. A number of studies have utilized the sequential three-state model to analyze the ligand-binding process, which can be written as (Henry et al., 1983):



where state A is the ligand bound state, state B is the intermediate state in which the ligand is not bound to the heme iron but still trapped within the protein, and state S is the ligand free state in solution (Carver et al., 1990; Henry et al., 1983; Lambright et al., 1989). The energy barriers for the ligand binding process ($A \leftrightarrow B$) and the diffusion process ($B \leftrightarrow S$) are referred to as the inner and the outer barrier, respectively.

To investigate the pathways for ligand binding, ligand-binding kinetics (Carver et al., 1990; Gibson et al., 1992; Huang and Boxer, 1994; Olson and Phillips, 1996; Scott and Gibson, 1997), time-resolved x-ray crystallography

(Brunori et al., 2000; Hartmann et al., 1996; Ostermann et al., 2000; Schlichting et al., 1994; Srajer et al., 1996), and molecular dynamics calculations (Carlson et al., 1996; Case and Karplus, 1979; Elber and Karplus, 1990; Ma et al., 1997; Meller and Elber, 1998) have been used, of which results have gradually agreed in suggesting that the dissociated ligands initially move away from the iron into the protein to occupy a space surrounded by the residues Phe43, Ile107, Ile111, Leu29, Val68, and His64 and the heme group, not directly toward the exterior.

Recently, based on the extensive study on the geminate O₂ rebinding of various sperm whale myoglobin mutants in the presence and absence of xenon, Scott and Gibson (1997) proposed that, after the initial movement, some photodissociated ligands would be trapped in xenon site 4, surrounded by Gly25, Ile28, Leu29, Val68, and Ile107 in the distal pocket. The time-resolved crystallographic data have also shown CO molecules, 4 ns after photodissociation, in or around xenon site 4, which disappear after 1 μ s (Srajer et al., 1996). These results strongly suggest that the xenon site 4 is a docking site for the ligand in the ligand-binding intermediate state, which is one of the crucial positions for the ligand migration in myoglobin.

Among the amino acid residues defining the xenon site 4, functional roles of Leu29 and Val68 in ligand binding have been focused on by many research groups including us (Adachi et al., 1992; Carver et al., 1990; Egeberg et al., 1990; Gibson et al., 1992; Ikeda-Saito et al., 1993; Krzywdka et al., 1998; Olson and Phillips, 1996; Quillin et al., 1995; Scott and Gibson, 1997; Smerdon et al., 1991; Uchida et al., 1997). The mutation at Leu29 to a less bulky amino acid residue, alanine, substantially decreased the geminate yield and the rebinding rate constant, proposing that the increased space accessible to the ligands lowers the free energy of the ligand-binding intermediate state in myoglobin (Gibson et al., 1992). Replacement of Leu29 with less hydrophobic

Received for publication 31 July 2000 and in final form 14 December 2000.

T. Uchida's present address: Institute for Molecular Science, Okazaki National Research Institutes, Myodaiji-cho, Okazaki 444-8585, Japan.

Address reprint requests to Dr. Isao Morishima, Department of Molecular Engineering, Graduate School of Engineering, Kyoto University, Kyoto 606-8501, Japan. Tel.: 81-75-753-5921; Fax: 81-75-751-7611; E-mail: morisima@mds.moleng.kyoto-u.ac.jp.

© 2001 by the Biophysical Society

0006-3495/01/03/1507/11 \$2.00

amino acid residues such as serine and glycine also reduced geminate yield and rate constants, due to the stabilization of noncoordinated distal water molecules near the ligand-binding site (Uchida et al., 1997).

On the other hand, introduction of isoleucine to position 68 remarkably increased both the free energies of the ligated state and the inner kinetic barrier, due to the severe steric hindrance between the side chain and ligand (Carver et al., 1990). However, the mutation to leucine, of which side-chain volume is the same as that of isoleucine, did not influence the free energies of the ligated state and the inner barrier, but significantly lowered the kinetic barrier for the ligand migration and increased the affinity for O₂ by displacing the distal pocket water molecule (Carver et al., 1990). More bulky substitution for Val68, Val→Phe, accelerated the geminate recombination and increased the geminate yield, indicating that the limited space available for photodissociated ligand raised the free energies of the intermediate state and the outer barrier by unfavorable steric interactions (Quillin et al., 1995).

Among the amino acid residues constructing the xenon site 4, Ile107 had the third largest number of collisions with the photodissociated ligand next to those of Leu29 and Val68 as shown by the molecular dynamic simulation (Elber and Karplus, 1990) and is another possible amino acid residue to interact with photodissociated ligands in the ligand-binding intermediate state (Lim et al., 1997; Srajer et al., 1996). The molecular dynamics study proposed (Elber and Karplus, 1990) a ligand pathway through hydrophobic channels between the E and B or H and G helices and raised the possibility that the space near Ile107 would be a ligand pathway in myoglobin. Recently, time-resolved x-ray crystallography studies indicated that ligand migration occurs through some pathways involving docking sites (Chu et al., 2000; Ostermann et al., 2000). These results raise the possibility that the free space near Ile107 can also be available for the ligand escape and entry pathway between the heme cavity and solvent. However, a few studies have paid attention to the amino acid residue at the position 107 (Quillin et al., 1995; Scott and Gibson, 1997) because Ile107 is located on the G helix near the vinyl group of the heme, the opposite site to the exit for solvent (Fig. 1), and far from the distal histidine and distal pocket water molecule. Scott and Gibson (1997) prepared four Ile107 mutants (I107A, I107V, I107L, and I107W) and characterized their geminate ligand-binding properties, but overall kinetic data have not yet been reported. The functional significance of Ile107, particularly the steric effects, on the ligand binding and pathway have not yet extensively been examined.

To gain insights into the steric effects of the side chain at position 107 on the ligand binding of myoglobin, some site-specific mutants of human myoglobin have been prepared, in which isoleucine 107 is replaced by amino acid residues having different steric hindrances, such as alanine, valine, leucine, and phenylalanine. By applying the empir-

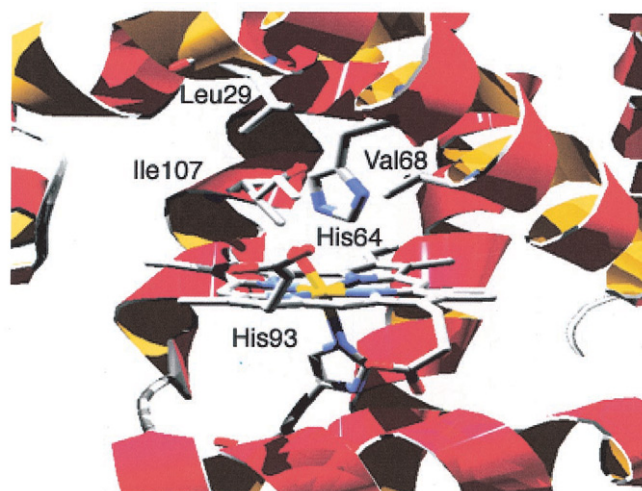


FIGURE 1 Heme environmental structure of human myoglobin (Hubbard et al., 1990). The heme and some selected amino acid residues are shown.

ical two-barrier diagram to the ligand-rebinding kinetics, we determined energy diagrams for the ligand binding of the mutants and compared them with that of the wild-type (WT) protein. Combined with the structural characterization of the mutants by various spectroscopies, we clarified the significance of the steric hindrance at position 107 for the free energies of the ligand-binding intermediate and the activation states to discuss the ligand pathway in myoglobin.

EXPERIMENTAL PROCEDURES

Preparation and purification of proteins

The original expression vector of human myoglobin, pMb3 (pLcIIFXMb), is a gift from Varadarajan and Boxer (Varadarajan et al., 1985). All proteins used in this study have the Cys110→Ala mutation to avoid dimer formation during the purification (Varadarajan et al., 1989). The procedures for the site-directed mutagenesis are described in previous papers (Adachi et al., 1992; Kunkel, 1985; Varadarajan et al., 1989). DNA sequencing for all the mutants was performed by the DyeDeoxy Terminator method using ABI 373S DNA sequencer (Applied Biosystems, Foster City, CA). Purification of the recombinant wild-type and mutant proteins is described in previous papers (Adachi et al., 1992; Varadarajan et al., 1985). The mutant proteins were purified in the cyanomet form to avoid aggregation and denaturation.

Oxygenated protein samples were prepared by reducing cyanomet- or aquomet-myoglobin with a small amount of sodium dithionite. To remove excess sodium dithionite, the sample was quickly passed through a small Sephadex G-25 column equilibrated with Ar-saturated phosphate buffer. In the preparation of the carbonmonoxy adducts, cyanomet myoglobin was reduced by addition of a slight excess of sodium dithionite under CO atmosphere.

Electronic absorption and Fourier transform infrared (FTIR) spectra

Electronic absorption spectra of the purified proteins were recorded on a Shimadzu UV 2200 UV/visible spectrometer (Shimadzu, Kyoto, Japan) in

0.1 M phosphate buffer at pH 7.0. The sample concentration was $\sim 5 \mu\text{M}$, and the path-length of the UV cell was 1 cm.

The infrared (IR) spectra of the CO adducts of wild-type and mutant myoglobins were measured with a Bio-Rad FTS-30 spectrometer (Bio-Rad, Hercules, CA). The concentration of the protein sample was 2–3 mM in 0.1 M phosphate buffer at pH 7.0. About 40 μl of the sample solution was loaded onto the IR cuvette. The cuvette consists of two CaF_2 windows separated by a 0.1-mm spacer. The FTIR spectra reported in this paper were averages of 512 scans recorded at a resolution of 1 cm^{-1} .

Laser photolysis measurements

Milli-, micro-, and nanosecond photolysis experiments were carried out as previously reported (Adachi and Morishima 1989; Adachi et al., 1992; Uchida et al., 1997). A Q-switched Nd:YAG laser (Continuum, Surelite I-10, Santa Clara, CA) was used to generate 4–6-ns pulses at 532 nm. The voltage transmittance signals at 436 nm were collected on a digitizing oscilloscope (Tektronix, TDS320, Beaverton, OR) and then transferred to a NEC 98 computer for analysis. The sample concentration was $\sim 20 \mu\text{M}$. After the laser photolysis measurements, no spectral changes were observed for the oxygenated wild-type and mutant proteins. All kinetic measurements were carried out at least three times on different protein samples.

The standard deviations of the apparent rate constants introduced by a single exponential fitting were less than 1%. The bimolecular rate constants were estimated using the linear fitting of the apparent rate constants to the ligand concentrations, which includes errors of 1.5%. The larger errors were estimated in averaging observable kinetic parameters (k_{obs} , k_{g} , and ϕ_{g}) from three independent series of the measurements. Their standard deviations were $\sim 6\%$. The final error parameters for the observable kinetic parameters in the flash photolysis are, therefore, derived from averaging the observable kinetic parameters.

Dissociation rate constants of carbon monoxide and dioxygen

CO dissociation rate constants were measured by using the NO replacement method for the samples dissolved in 0.1 M phosphate at pH 7.0 and at 20°C (Lambright et al., 1989). The absorption change at 424 nm was monitored by a UV/visible spectrometer (Shimadzu UV-2200). NO-containing buffer was prepared by bubbling NO gas in the UV cell. About 30 μl of carbonmonoxy protein samples ($\sim 2 \text{ mM}$) were injected into the cell. The final sample concentration was $\sim 20 \mu\text{M}$. The decays were fitted by a single exponential curve (Lambright et al., 1989).

The kinetic measurements of the O_2 dissociation rate constants were determined by use of a stopped-flow spectrophotometer (Unisoku, Osaka, Japan) at 20°C in 0.1 M phosphate buffer at pH 7.0 (Antonini and Brunori, 1971). The concentration of the protein sample was $\sim 10 \mu\text{M}$. The ligand exchange reaction from O_2 to CO was followed by monitoring the absorbance change at 429 nm. The transmittance change was detected by a photomultiplier that is attached on a monochromator (Unisoku USP-501). The signal was digitized and accumulated using a two-channel oscilloscope (Tektronix TDS320). The data were transferred to an NEC 98 computer for further data analysis.

In the measurements of the dissociation rate constants, the standard deviation in the exponential fitting to the time course at each measurement was less than 2%. The larger deviations were observed for averaging the rate constant (k_{off}) from three independent measurements. The standard deviations in averaging were $\sim 8\%$. We listed the deviations in averaging the rate constant as the error parameters for the dissociation constants.

Kinetic model and analysis

Under the condition that the geminate rebinding can be fitted by a single exponential, the simple sequential three-state model (Henry et al., 1983)

has been used for the detailed analysis of the geminate ligand-binding process. The observable geminate rate constants (k_{g}), geminate yield (ϕ_{g}), bimolecular rebinding rate constants (k_{on}), and dissociation rate constants (k_{off}) are related to the rate constants for the elementary processes of the three-state sequential scheme by the following equations (Lambright et al., 1989):

$$k_{\text{g}} = k_{\text{BA}} + k_{\text{BS}} \quad (1)$$

$$\phi_{\text{g}} = k_{\text{BA}}/k_{\text{g}} = k_{\text{BA}}/(k_{\text{BA}} + k_{\text{BS}}) \quad (2)$$

$$k_{\text{on}} = k_{\text{SB}}\phi_{\text{g}} = k_{\text{SB}}k_{\text{BA}}/(k_{\text{BA}} + k_{\text{BS}}) \quad (3)$$

$$k_{\text{off}} = k_{\text{AB}}(1 - \phi_{\text{g}}), \quad (4)$$

where k_{XY} represents the forward rate constants from X to Y.

Thermodynamic parameters for the ligand-binding process

The free energy differences between two states are calculated using the following equation:

$$\Delta G = -RT \ln K \quad (5)$$

where K is the equilibrium constant.

The differences entropy and enthalpy are calculated using the van't Hoff equation:

$$\frac{d \ln K}{d(1/T)} = \frac{-\Delta H}{R} \quad (6)$$

$$\Delta G \equiv \Delta H - T\Delta S \quad (7)$$

Based on the following equation (Eyring equation), the kinetic barriers (ΔG^\ddagger) can be estimated:

$$k \equiv \kappa(k_{\text{B}}T/h) \times e^{-\Delta G^\ddagger/RT} \equiv A \exp(-\Delta G^\ddagger/RT), \quad (8)$$

where κ is the transmission coefficient and k_{B} and h represent the Boltzmann and Planck constants, respectively. Usually, the Eyring equation is effective only under the condition that the reactant is in equilibrium with the transition state. Due to the kinetic complexity of the ligand binding, the equilibrium along the reaction coordinate would be prevented, which leads to uncertainty of the thermodynamic parameters from Eq. 8. In this paper, the pre-exponential factors (A in Eq. 8) were set equal to 10^{10} s^{-1} (Carver et al., 1990):

$$\Delta G^\ddagger \equiv RT \ln(10^{10}/k) \quad (9)$$

Although the assumption of $A = 10^{10}$ in Eq. 9 might be arbitrary, the absolute values of pre-exponential factors do not affect the differences between the barrier heights for the mutant proteins and wild-type myoglobin. The errors for the thermodynamics were based on the standard deviations for the kinetic constants and their statistical treatments.

RESULTS

Structural characterization of the Ile107 mutants

To examine the heme environmental structure of the Ile107 mutants, we used various spectroscopies including absorption, resonance Raman, IR, and NMR spectra. The strong absorption band, the Soret band, has served as a marker for the polarity of the heme cavity, and increase of the polarity

shifts the Soret peak to the red-side (Laird and Skinner, 1989). In the carbonmonoxide adduct of wild-type human myoglobin, the Soret peak appeared at 422.9 nm (figure not shown), whereas the I107A, I107V, I107L, and I107F mutants exhibited their Soret peak at 422.1, 422.8, 423.2, and 422.3 nm, respectively (figure not shown). Although all the mutants showed slightly deviated peak positions, the deviations from the peak position of the wild-type protein were within 0.8 nm, indicating that the mutational perturbation on the polarity of the heme cavity is small.

Minor structural perturbations by the mutation at position 107 on the heme environment were also supported by the resonance Raman spectra. Close similarity of the resonance Raman spectra was encountered for the unliganded deoxygenated states of the mutants. In the deoxygenated state, the vibration modes of the porphyrin ring (ν_7 , ν_8 , and ν_9) and stretching mode between the axial histidine and heme iron were detected in the region between 200 and 450 cm^{-1} . In the spectra of the mutants, the Fe-His stretching mode was detected at 221 cm^{-1} as was in the wild-type protein, and the vibration modes of the porphyrin ring for the mutants were observed almost at the same positions as those for the wild-type protein (data not shown). Close spectral similarity between the mutants and wild-type myoglobin was also observed for the NMR spectra of the cyanide and carbon monoxide adducts. Although some of the signal positions were shifted (less than 1.3 ppm) by the mutation, the spectral perturbations were not so drastic, implying that the heme environmental structure in the mutants would be the same as that in the wild-type protein (data not shown).

In sharp contrast to the electronic absorption, resonance Raman, and NMR spectra of the mutants, the IR spectra, a sensitive probe of the electrostatic potentials near the ligand-binding site (Phillips et al., 1999), of the I107 mutants were distinctly different from that of wild-type myoglobin as displayed in Fig. 2. Previous studies have revealed that the stretching mode for heme-bound CO can be decomposed into three conformers (Oldfield et al., 1991). As the dotted lines show in Fig. 2, the peak at 1946 cm^{-1} with a shoulder around 1941 cm^{-1} is the major conformer in wild-type myoglobin, which has been assigned to the A_1 conformer (Oldfield et al., 1991). The other peaks around 1970 and 1938 cm^{-1} were also observed for some mutants, which are assigned to the A_0 and A_3 conformers, respectively (Oldfield et al., 1991). The A_0 conformer has been considered to have a configuration in which bound CO has no electrostatic interactions and the distal His swings away from the heme iron, whereas the conformer A_3 has more positive charges near the oxygen atom of bound CO than the conformer A_1 and the distal His is located close to the heme iron (Li et al., 1994; Morikis et al., 1989; Oldfield et al., 1991; Vojtechovsky et al., 1999).

In the IR spectra of the I107L, I107V, and I107A mutants, the A_1 conformer was still the major conformer, but a slight increase of the A_0 conformer was detected. Although

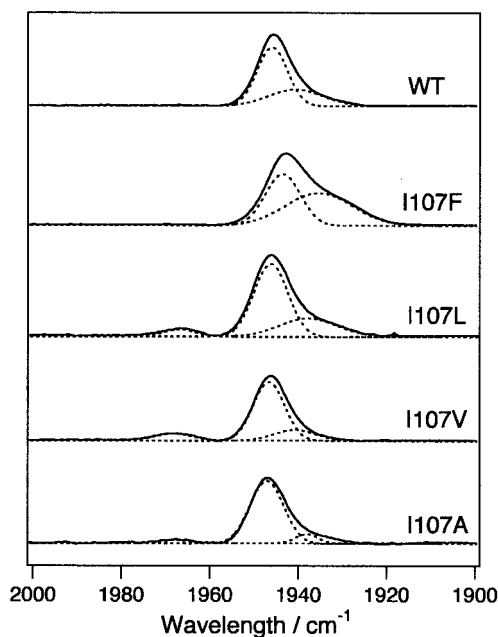


FIGURE 2 FTIR spectra of the C-O stretching region of wild-type and mutant myoglobins in the carbonmonoxy forms. Components are shown as broken lines. Each sample contains ~ 2.5 mM protein in 0.1 M phosphate buffer adjusted to pH 7.0.

the increase of the A_0 conformer at the expense of the conformer A_1 suggests the diminution of positive charges near bound CO, the spectral changes were less drastic compared with that by the mutation at Leu29 (Li et al., 1994). Thus, the alterations of the heme environments by the mutation at position 107 to leucine, valine, or alanine are rather small.

On the other hand, the mutational effects on the IR spectra for the I107F mutant were different from those for other mutants. The population of the A_3 conformer was increased up to 55% in the mutant, indicative of the more positively charged environments around ligated CO. Such an increase in the A_3 conformer was also reported for the V68F and L29F mutants that have a bulky phenylalanine residue inside the heme pocket (Li et al., 1994). As suggested by the x-ray structure of these mutants, the positive edge of the phenylalanine can interact with bound CO (Quillin et al., 1995), leading to the characteristic low-wavenumber stretching band for bound CO. The positions of the IR stretching band and population of the conformers for the wild-type and mutant proteins are summarized in Table 1.

O₂ bimolecular rebinding and dissociation process

As previously revealed (Chatfield et al., 1990), the ligand rebinding by laser flash photolysis for hemoproteins often shows at least two well-separated kinetic processes. One is

TABLE 1 Peak positions of IR stretching band for the carbonmonoxy complex of WT and mutant myoglobins

	A ₀	A _{1,2} (cm ⁻¹ (%))	A ₃
I107F	ND	1943 (45)	1935 (55)
WT	ND	1946 (100)	ND
I107L	1967 (6)	1946 (94)	ND
I107V	1968 (10)	1947 (72)	1938 (18)
I107A	1968 (4)	1947 (96)	ND

The values in parentheses indicate the population of conformers.

the slower phase, the bimolecular process, and the other is the geminate process, which is much faster than the bimolecular process. Typical time courses for the bimolecular rebinding in wild-type and mutant myoglobins are shown in Fig. 3. These time courses can be fitted by a single exponential, and the apparent association rate constants (k_{on}) are compiled in Table 2.

As clearly shown in Table 2, k_{on} correlated with the side-chain volume at position 107. The I107F mutant, which has the most bulky side chain (side-chain volume of 135 Å³) at position 107, exhibited the slowest bimolecular rebinding rate constant (10.1 μM⁻¹ s⁻¹), whereas the most accelerated rebinding rate constant (30.4 μM⁻¹ s⁻¹) was observed for the alanine-substituted I107A mutant (side-chain volume of 67 Å³). The rebinding rate constant for the valine (side-chain volume of 105 Å³) substituted mutant (22.0 μM⁻¹ s⁻¹) was smaller than that of the I107A mutant but larger than that of wild-type myoglobin (16.0 μM⁻¹ s⁻¹; side-chain volume of 124 Å³). The isovolume substitution

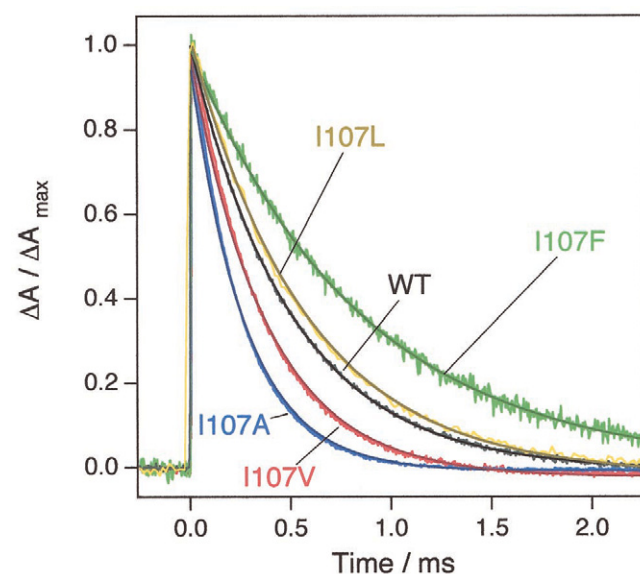


FIGURE 3 Time courses for the millisecond rebinding of O₂ to wild-type and mutant myoglobins dissolved in 0.1 M phosphate buffer at pH 7.0. The absorbance changes for the bimolecular process have been normalized to unity. Reactions were monitored at 436 nm.

for leucine gives almost the same rebinding rate constant (15.2 μM⁻¹ s⁻¹) as that of wild-type myoglobin.

The correlation was also manifested in the dissociation rate constant (k_{off}) for oxygen as listed in the fourth column of Table 2. The dissociation reaction was accelerated by the decrease of the side-chain volume as listed in Table 2. It is also interesting that the overall affinity, the equilibrium constant for the oxygen binding (K), is almost independent of the volume of the side chain, due to the compensation effects between the association and dissociation rate constants.

O₂ geminate rebinding process

Another kinetic phase in the ligand-binding reaction is the geminate process. The geminate rebinding is observed for nanosecond photolysis, and the typical half-times are less than a few microseconds (Henry et al., 1983), whereas that for the bimolecular rebinding is nearly 1 ms (Antonini and Brunori 1971). The O₂ rebinding time course for wild-type myoglobin in the microsecond region is shown in Fig. 4. As reported in a previous study (Chatfield et al., 1990), the geminate O₂ rebinding in myoglobin has two relaxations: the rate constant of the initial fast phase is 33.7 μs⁻¹, and that of the slower and smaller phase is 5.43 μs⁻¹. In the time course for the wild-type protein, the fitting by a single exponential was systematically deviated from the observed decay (middle panel of Fig. 4), but the residuals from the two-exponential fitting (top panel of Fig. 4) were almost random, implying that the ligand binding for human myoglobin under our condition is biphasic. The rate constants for the fast (k_{g1}) and slow (k_{g2}) phases of the geminate rebinding were 37 and 7.4 μs⁻¹, respectively, corresponding to those previously reported (Chatfield et al., 1990). The geminate yields were estimated as 0.45 (ϕ_{g1}) and 0.002 (ϕ_{g2}) for the fast and slow phases, respectively.

On the other hand, the geminate rebinding for the mutants can be fitted by a single exponential as exemplified in Fig. 5. The residuals from single-exponential fitting (top panel of Fig. 5) in the time course for the I107F mutant were randomly distributed, and no systematic deviations were observed. By the single-exponential fitting for the time courses, the geminate rebinding rate constants (k_g) and yields (ϕ_g) for the mutants were estimated as summarized in Table 2. Although both the geminate rate constant and yield depended on the side-chain volume of position 107, the correlation was not linear. The most bulky I107F mutant had the largest geminate rate constant, 22.4 μs⁻¹, whereas the slowest geminate rebinding rate constant (7.7 μs⁻¹) was obtained for the I107A mutant. The rate constant for the I107V was in the middle of the other two mutants, but its geminate rebinding rate constant was larger than that of the I107L mutant.

It is not so simple to directly compare the kinetic properties for the geminate rebinding of the mutants with those

TABLE 2 Observed kinetic parameters for O₂ binding for WT and mutant myoglobins

	Side-chain volume (Å ³)	k_{on} (μM ⁻¹ s ⁻¹)	k_{off} (s ⁻¹)	K (μM ⁻¹)	k_g (μs ⁻¹)	ϕ_g
I107F	203.4	10.1 ± 0.3	5.1 ± 0.3	2.00 ± 0.17	22.4 ± 0.4	0.73 ± 0.01
WT	168.8	16.0 ± 0.7	15.6 ± 0.8	1.02 ± 0.10	18.2 ± 0.2	0.45 ± 0.02
I107L	167.9	15.2 ± 0.3	18.8 ± 1.1	0.81 ± 0.06	9.4 ± 0.3	0.32 ± 0.02
I107V	141.7	22.0 ± 0.2	19.0 ± 0.6	1.16 ± 0.05	12.2 ± 0.3	0.24 ± 0.01
I107A	91.5	30.4 ± 0.9	23.0 ± 1.7	1.32 ± 0.14	7.7 ± 0.1	0.39 ± 0.01

The values of side-chain volume are from Chothia (1975).

of wild-type myoglobin, because the geminate O₂ rebinding in the mutants was monophasic and that in wild-type myoglobin was biphasic. However, because the fraction of the slow phase in wild-type myoglobin is small, it would be an acceptable approximation that we adopt a single-exponential fitting to the time course for the geminate rebinding of wild-type myoglobin (Krzywda et al., 1998). As the previous study reported (Carlson et al., 1996), the single-exponential fitting to the geminate O₂ rebinding provides a reasonably accurate mathematical description of the kinetics of ligand binding in the time scales greater than tens of nanoseconds. The kinetic parameters analyzed by the single-exponential fitting, k_g and ϕ_g , for wild-type myoglobin are also listed in Table 2. The geminate rebinding rate constant for wild-type myoglobin is larger than that of the I107V mutant and smaller than that of the I107F mutant.

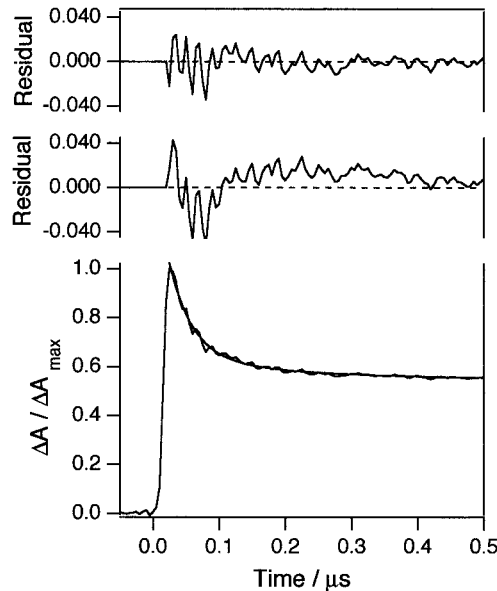


FIGURE 4 Time courses for the geminate rebinding of O₂ to wild-type myoglobin dissolved in 0.1 M phosphate buffer at pH 7.0. The upper and middle traces are the residuals from the double-exponential and the single-exponential fittings, respectively, to the observed time course shown as the lower trace. Reaction was monitored at 436 nm.

Kinetic model and analysis for O₂ rebinding process

Under the condition that the geminate rebinding can be fitted by a single exponential, the simple sequential three-state scheme has been utilized for the detailed analysis of the ligand-binding process (Morikis et al., 1989). Therefore, the observed geminate rate constants (k_g), geminate yield (ϕ_g), bimolecular rebinding rate constants (k_{on}), and dissociation rate constants (k_{off}) are related to the rate constants for the elementary processes of the three-state sequential scheme by the Eqs. 1–4 (Lambright et al., 1989). The resultant rate constants of the elementary processes and equilibrium constants for the three-state model are listed in Table 3. To clarify the mutational effects on the energy

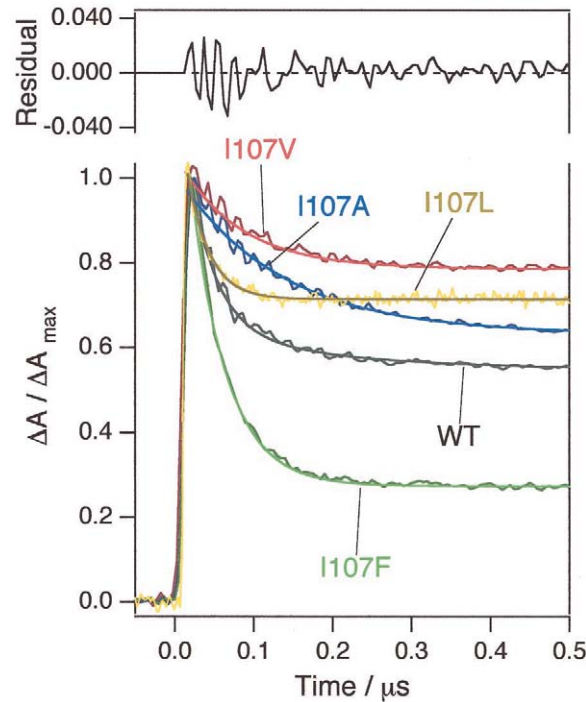


FIGURE 5 Time courses for the geminate rebinding of O₂ to mutant proteins dissolved in 0.1 M phosphate buffer at pH 7.0. The absorbance changes were monitored at 436 nm. The residuals from the single-exponential fit to the time course of I107F are presented as the upper trace.

TABLE 3 Calculated parameters for O₂ binding for WT and mutant myoglobins

	Side-chain volume (Å ³)	k_{AB} (s ⁻¹)	k_{BA} (μs ⁻¹)	K_{AB} (×10 ⁻⁶)	k_{BS} (μs ⁻¹)	k_{SB} (μM ⁻¹ s ⁻¹)	K_{SB} (M ⁻¹)	K_{SA} (μM ⁻¹)
I107F	203.4	18.7 ± 1.2	16.4 ± 0.5	1.1 ± 0.1	6.1 ± 0.9	13.8 ± 0.2	2.3 ± 0.4	2.0 ± 0.2
WT	168.8	28.4 ± 2.5	8.19 ± 0.4	3.5 ± 0.5	10.0 ± 0.5	35.6 ± 0.9	3.6 ± 0.3	1.0 ± 0.1
I107L	167.9	27.6 ± 3.3	3.01 ± 0.3	9.2 ± 2.0	6.4 ± 0.6	47.5 ± 0.6	7.4 ± 0.8	0.8 ± 0.1
I107V	141.7	24.9 ± 1.3	2.93 ± 0.1	8.5 ± 0.9	9.3 ± 0.5	91.7 ± 0.8	9.9 ± 0.6	1.2 ± 0.1
I107A	91.5	37.7 ± 3.4	3.01 ± 0.1	12.6 ± 1.5	4.7 ± 0.2	77.9 ± 1.9	16.6 ± 1.1	1.3 ± 0.1

The values of side-chain volume are from Chothia (1975).

potentials for the O₂ binding in myoglobin, we estimate the free energy differences between the different states (ΔG) and their activation energies (ΔG^\ddagger) by Eqs. 5 and 8, respectively. Several free energy differences and activation energies in the three-state model for the ligand binding of the wild-type and mutant proteins are listed in Table 4 and the empirical two-barrier diagram is shown in Fig. 6. In this diagram, the free energy of the unliganded state with a free ligand in solution (state S) was arbitrarily assigned to 0 and that of the ligand-binding intermediate state B, ΔG_{SB} , was calculated by $-RT\ln(K_{SB})$. $-RT\ln(K_{SA})$ was used for estimation of the free energy for the liganded state (state A), ΔG_{SA} (Antonini and Brunori 1971; Carver et al., 1990; Lambright et al., 1989). The assignment of absolute values to the barrier heights is more arbitrary, but the relative values were defined by measured geminate rebinding parameters, k_{BA} and k_{BS} . The inner (bond formation) and outer (ligand migration) barriers were estimated by $\Delta G_{BA}^\ddagger = RT\ln(10^{10}/k_{BA})$ and $\Delta G_{BS}^\ddagger = RT\ln(10^{10}/k_{BS})$, respectively (Carver et al., 1990). We also determined the enthalpy (ΔH) and entropy (ΔS) for the elementary process in the three-state model by measuring the rate constants at 283 K, 293 K, and 303 K and using Eqs. 6 and 7. The values of ΔH_{SB} and ΔS_{SB} for WT, I107F, I107L, I107V, and I107A are compiled in Table 5.

CO bimolecular rebinding and dissociation process

In sharp contrast to the O₂ binding, the CO binding to the mutants does not show a clear relationship with the steric hindrance at the side chain of position 107. As illustrated in Fig. 7, the time courses for the CO bimolecular rebinding process in the mutants were not so drastically deviated from

that of wild-type myoglobin, compared with those for the O₂ bimolecular rebinding process. The CO bimolecular rebinding time courses for the I107A, I107V, and I107V mutants were monophasic, which could be fitted by a single exponential, and the I107F mutant exhibited a biphasic time course. The apparent association rate constants (k_{on}) for the mutants were in the range between 0.70 and 1.39 μM⁻¹ s⁻¹. The dissociation rate constants (k_{off}) also showed slight dependence of the side-chain volume at position 107, and two relaxations were detected for the I107F and I107L mutants. The kinetic parameters for the CO rebinding are summarized in Table 6.

DISCUSSION

Steric effect of Ile107 on the ligand bound state

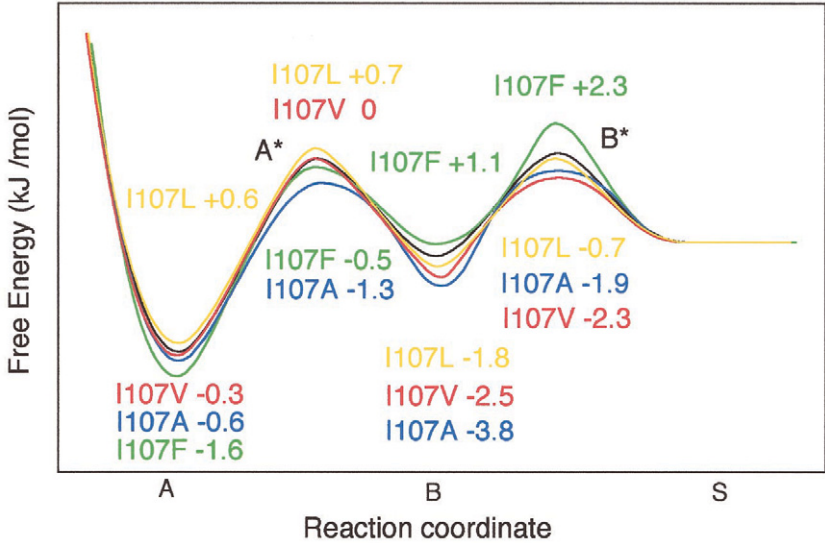
As clearly shown in the various spectroscopic and kinetic results, perturbations on the ligand bound state (state A) by the mutations at Ile107 are rather small. The deviations of the free energy difference between the ligand bound and ligand free states (ΔG_{SA}) in the mutants are less than 1.6 kJ mol⁻¹. The minor effects of the mutations at Ile107 on the heme environmental structure are evident by the absorption and resonance Raman spectra of the mutants, which have close similarity to those of wild-type myoglobin.

It is not so surprising that the amino acid substitution at position 107 causes only minor perturbation on the heme environmental structure in the ligand bound state, because Ile107 is located far way from the heme iron. Although the CO stretching modes for the I107F mutant indicate the interactions of the phenyl ring and heme-bound CO, the distance from the heme plane to the phenyl ring protons of Phe107 would be more than 6.8 Å. Combined with the

TABLE 4 Free energy and free energy of activation for O₂ binding for WT and mutant myoglobins

	ΔG_{AB}^\ddagger (kJ/mol)	ΔG_{BA}^\ddagger (kJ/mol)	ΔG_{AB} (kJ/mol)	ΔG_{BS}^\ddagger (kJ/mol)	ΔG_{SB}^\ddagger (kJ/mol)	ΔG_{SB} (kJ/mol)	ΔG_{SA} (kJ/mol)	$\Delta G_{SB} + \Delta G_{BA}^\ddagger$ (kJ/mol)
I107F	49.0 ± 3.2	15.6 ± 0.5	33.3 ± 3.1	18.1 ± 2.7	16.0 ± 0.3	-2.0 ± 0.3	-35.3 ± 2.9	13.6 ± 0.8
WT	47.9 ± 4.2	17.3 ± 0.8	30.6 ± 4.0	16.8 ± 0.9	13.7 ± 0.4	-3.1 ± 0.2	-33.7 ± 3.3	14.2 ± 1.0
I107L	48.0 ± 5.7	19.8 ± 1.9	28.3 ± 6.0	17.9 ± 1.6	13.0 ± 0.2	-4.9 ± 0.5	-33.1 ± 2.6	14.9 ± 2.4
I107V	48.3 ± 2.6	19.8 ± 1.0	28.4 ± 2.9	17.0 ± 0.9	11.4 ± 0.1	-5.6 ± 0.3	-34.0 ± 1.4	14.2 ± 1.3
I107A	47.3 ± 4.3	19.8 ± 0.6	27.5 ± 3.3	18.7 ± 0.7	11.8 ± 0.3	-6.8 ± 0.4	-34.3 ± 3.6	12.9 ± 1.0

FIGURE 6 Free energy diagrams for the O₂ rebinding reaction for wild-type and mutant myoglobins. A is the bound state, B is the intermediate state, and S is the ligand free state in solution. A* is the activation state for the bond formation process, and B* is the activation state for the ligand migration process



structural and kinetic properties of the mutants, we can conclude that the steric and electrostatic effects of the side chain at position 107 on ΔG_{SA} are not so prominent.

Steric effect of Ile107 on the bond formation process and its activation state

The free energy difference for the bond formation reaction, ΔG_{AB} , clearly depends on the side-chain volume at position 107 (Table 4). The I107F mutant having the bulky phenyl ring at position 107 showed a larger ΔG_{AB} (33.3 kJ mol⁻¹) than wild-type myoglobin (30.6 kJ mol⁻¹), whereas a smaller ΔG_{AB} (27.5 kJ mol⁻¹) was obtained for the I107A mutant. However, the activation energy for the ligand-binding intermediate state from the ligand bound state (ΔG_{AB}^\ddagger), the free energy for the ligand bound state (ΔG_{SA}), and the free energy difference between the activation state for the bond formation process (A*) and the unliganded state, ($\Delta G_{BA}^\ddagger + \Delta G_{SB}$), are almost independent of the side-chain volume at position 107. Thus, the side-chain volume dependence of ΔG_{AB} can primarily be ascribed to that of the free energy for the ligand intermediate state B (ΔG_{SB}), not to the activation energy for the bond formation process.

TABLE 5 Free energy, enthalpy, and entropy for O₂ binding for WT and mutant myoglobins at 293 K

	Side-chain volume (Å ³)	ΔG_{SB} (kJ/mol)	ΔH_{SB} (kJ/mol)	ΔS_{SB} (J/mol K)
I107F	203.4	-2.0 ± 0.3	9 ± 1.8	38 ± 7.3
WT	168.8	-3.1 ± 0.2	17 ± 0.8	70 ± 3.7
I107L	167.9	-4.9 ± 0.5	11 ± 2.4	55 ± 9.9
I107V	141.7	-5.6 ± 0.3	14 ± 2.7	67 ± 10
I107A	91.5	-6.8 ± 0.4	13 ± 1.5	68 ± 6.5

The values of side-chain volume are from Chothia (1975).

It is quite interesting that the mutation at Val68 or Leu29, both of which form the xenon site 4 as does Ile107, showed the drastic changes of ΔG_{BA}^\ddagger (Carver et al., 1990; Quillin et al., 1995). The introduction of a large phenyl ring into the ligand-binding site in the V68F mutant accelerated the bond formation rate constant, corresponding to more than 7.1 kJ mol⁻¹ decrease of ΔG_{BA}^\ddagger . The barrier for the bond formation is lowered in part by the increased free energy of the geminate state due to less volume available for the dissociated ligand and to the small steric barrier for the ligand return (Carver et al., 1990). Although a decrease of ΔG_{BA}^\ddagger was observed for the I107F mutant, the change of ΔG_{BA}^\ddagger

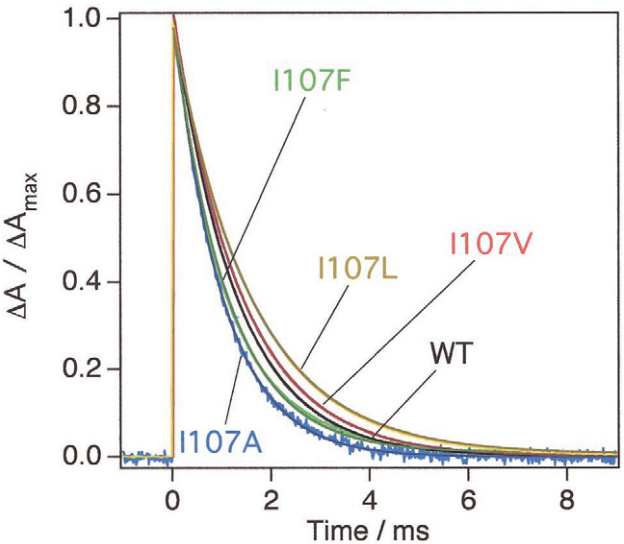


FIGURE 7 Time courses for the millisecond rebinding of CO to wild-type and mutant myoglobins dissolved in 0.1 M phosphate buffer at pH 7.0. The absorbance changes for the bimolecular process have been normalized to unity. Reaction was monitored at 436 nm.

TABLE 6 Observed kinetic parameters for CO binding for WT and mutant myoglobins

	Side-chain volume (\AA^3)	k_{on} ($\mu\text{M}^{-1} \text{s}^{-1}$ (%))	k_{off} (s^{-1} (%))	K (μM^{-1})
I107F	135	1.39 ± 0.05 (53) 0.70 ± 0.01 (47)	0.009 ± 0.000 (78) 0.026 ± 0.003 (22)	84
WT	124	0.84 ± 0.01	0.019 ± 0.001	44
I107L	124	0.64 ± 0.02	0.021 ± 0.001 (87) 0.059 ± 0.006 (13)	25
I107V	105	0.78 ± 0.01	0.017 ± 0.001	46
I107A	67	1.10 ± 0.04	0.014 ± 0.001	79

The values of side-chain volume are from Chothia (1975).

The values in parentheses indicate the amplitudes of each phase.

(1.6 kJmol^{-1}) was much smaller. Such a prominent effect can be attributed to the location of the side chain at position 68. The distances between protons of the side chain of Val68 and the heme iron are less than 4.9 \AA , which is much closer than those of Ile107 (6.4 \AA). On the other hand, some substitutions of Leu29, of which the side chain is located far from the heme iron (7.7 \AA), induced remarkable reduction of the association rate constant in myoglobin, corresponding to the increase of $\Delta G_{\text{BA}}^\ddagger$ (Adachi et al., 1992). Despite the small side-chain volume of the substituted amino acid residues, the L29G and L29S mutants have quite slow ligand-binding rate constants due to the stabilization and/or introduction of the water molecules (Uchida et al., 1997).

Because the side chain of the Ile107 is too far away to interact directly bound ligands and the mutants we prepared in this study have almost the same hydrophobicities at position 107 as that of wild-type myoglobin, it is reasonably inferred that the alterations of the side chain at position 107 would not so drastically perturb the steric hindrance around the ligand-binding site nor stabilize the distal water molecules, resulting in minor perturbation on the activation state for the bond formation process. Such minor effects of the mutation of Ile107 on the bond formation are also confirmed in the CO rebinding for the mutants. As summarized in Table 6, the apparent association rate constants for the CO rebinding in the I107 mutants show no correlation with the side-chain volume, indicating that the activation energy for the bond formation process is independent of the side-chain volume at position 107.

Steric effect of Ile107 on the ligand-binding intermediate state

In sharp contrast to the minor effects of the mutation on the ligand bound state and bond formation process, the volume change of the side chain at position 107 substantially affected the free energy of the ligand binding intermediate state, ΔG_{SB} . In the bulky I107F mutant, ΔG_{SB} is increased by 1.1 kJ mol^{-1} , whereas less bulky I107 mutants, I107V and I107A mutants, have reduced ΔG_{SB} (2.5 and 3.8 kJ

mol^{-1} , respectively, from ΔG_{SB} of wild-type myoglobin) as displayed in Fig. 6. Lowered ΔG_{SB} with decreasing volume of the side chain at position 107 implies that the enlargement of the space around Ile107 contributes to the stabilization of the ligand-binding intermediate state (Quillin et al., 1995). In other words, the space around Ile107 can be available as the ligand-docking site for the ligand-binding intermediate state.

However, the leucine-substituted mutant, of which side-chain volume at position 107 is identical to that of wild-type myoglobin, showed lower ΔG_{SB} than wild-type myoglobin, which was close to that in the valine-substituted mutant. Such a different behavior between the leucine and isoleucine substitutes is also found for the Val68 mutants (Carver et al., 1990). Quillin et al. (1995) pointed out that the *iso*-butyl side chain of leucine is more flexible to accommodate bound ligands without extensive steric hindrance than the *sec*-butyl side chain of isoleucine. Thus, ΔG_{SB} would depend not only on the side-chain volume of position 107 but also on the flexibility of the side chain.

To gain further insights into the interactions between the ligand and the side chain at position 107, we determined thermodynamic parameters, ΔS_{SB} and ΔH_{SB} , the formation entropy and enthalpy of the ligand-binding intermediate state (Table 5). All of the mutants and wild-type myoglobin exhibited small positive enthalpy and large positive entropy, indicating that the reaction from the unliganded state to the ligand-binding intermediate state is an entropy-driven reaction. As summarized in Table 5, regardless of the steric hindrance of the side chain, the mutants have reduced ΔH_{SB} , compared with that of wild-type myoglobin. Because ΔH_{SB} can be divided into the favorable hydrophobic interaction and unfavorable steric interaction between the ligand and surrounding amino acid residues, decreased ΔH_{SB} by the mutations would be ascribed to the increase of the favorable hydrophobic interaction and/or the decrease of the steric repulsion. On the other hand, a substantial decrease of ΔS_{SB} was observed for the I107F mutant. As previously proposed (Quillin et al., 1995), the diminution of the distal pocket volume by the introduction of a bulky amino acid into the heme cavity causes the decrease of the entropy for noncoordinate ligand because of the limited space available to move (Quillin et al., 1995). In the I107F mutant, the introduction of bulky phenyl group into the position of 107 would reduce the space available to the photodissociated ligands, resulting in a lowering of the entropy.

Steric effect of Ile107 for the ligand migration process and its activation state

The side-chain volume at position 107 also significantly affected the free energy of the activation state B^* ($\Delta G_{\text{SB}}^\ddagger$) in Fig. 6. The value of $\Delta G_{\text{SB}}^\ddagger$ for the I107F mutant was increased by 2.3 kJ mol^{-1} , compared with that of the wild type, whereas the I107V and I107A mutants exhibited sub-

stantial decrease in the ΔG_{SB}^\ddagger value by -2.3 and -1.9 kJ mol $^{-1}$, respectively. ΔG_{SB}^\ddagger for the isovolume leucine mutant is almost identical to that of wild-type myoglobin. The increase of the side-chain volume enhanced the kinetic barrier from the unliganded state to the ligand-binding intermediate state and destabilized the activation state B*. The size of the side chain at position 107, therefore, has a significant role in formation of the activation state for the ligand migration, and a space around Ile107 would be shrunk in the activation state, suggesting that the space near Ile107 is occupied by the photodissociated ligand in the activation state. Because the position of the photodissociated ligand in the activation state for the ligand migration can be considered as a critical position for the ligand pathway in myoglobin (Quillin et al., 1995; Rohlfis et al., 1990), the present kinetic results suggest that the photodissociated ligand migrates from the heme iron to solvent through the space near Ile107 in the protein, supporting the possible ligand pathway through the protein interior proposed by the molecular simulation (Elber and Karplus 1990).

In summary, the side-chain volume at position 107 is one of the factors to affect the free energy of the ligand-binding intermediate state and activation energy for the ligand migration process. The lowered free energy of the ligand-binding intermediate state with decreasing the side-chain volume at position 107 implies that the space near Ile107 can accommodate photodissociated ligands as a ligand-docking site, and acceleration for the ligand migration process by reducing the size of the side chain at position 107 allows us to propose that the free space near Ile107 can also be available for the ligand escape and entry pathway between the heme cavity and solvent. Because Ile107 is located in the protein interior of myoglobin, our results strongly suggest the ligand pathway through hydrophobic interior channels is formed by the E and B or H and G helices (Elber and Karplus 1990).

We are grateful to Prof. S. G. Boxer and Dr. R. Varadarajan (Stanford University) for a gift of the expression vector of the human myoglobin gene. We are also indebted to Prof. T. Kitagawa (Institute for Molecular Science) for kind permission to use his resonance Raman observing system.

This work was supported by Grant-in-Aid for Science Research on Priority Areas, Molecular Biometallics, from the Ministry of Education, Science, Sports and Culture (08249102) to I.M. H.I. and T.U. were supported by the fellowship of Japan Society for Promotion of Science to Japanese young scientists.

REFERENCES

- Adachi, S., and I. Morishima. 1989. The effects of pressure on oxygen and carbon monoxide binding kinetics for myoglobin. *J. Biol. Chem.* 264: 18896–18901.
- Adachi, S., N. Sunohara, K. Ishimori, and I. Morishima. 1992. Structure and ligand binding properties of leucine 29(B10) mutants of human myoglobin. *J. Biol. Chem.* 267:12614–12621.
- Antonini, E., and M. Brunori. 1971. Hemoglobin and Myoglobin in Their Reactions with Ligands. North-Holland, Amsterdam.
- Brunori, M., B. Vallone, F. Cutruzzola, C. Travaglini-Allocatelli, J. Berendzen, K. Chu, R. M. Sweet, and I. Schlichting. 2000. The role of cavities in protein dynamics: crystal structure of a photolytic intermediate of a mutant myoglobin. *Proc. Natl. Acad. Sci. U.S.A.* 97: 2058–2063.
- Carlson, M. L., R. M. Regan, and Q. H. Gibson. 1996. Distal cavity fluctuations in myoglobin: protein motion and ligand diffusion. *Biochemistry*. 35:1125–1136.
- Carver, T. E., R. J. Rohlfis, J. S. Olson, Q. H. Gibson, R. S. Blackmore, B. A. Springer, and S. G. Sligar. 1990. Analysis of the kinetic barriers for ligand binding to sperm whale myoglobin using site-directed mutagenesis and laser photolysis techniques. *J. Biol. Chem.* 265: 20007–20020.
- Case, D. A., and M. Karplus. 1979. Dynamics of ligand binding to heme proteins. *J. Mol. Biol.* 132:343–368.
- Chatfield, M. D., K. N. Walda, and D. Magde. 1990. Activation parameters for ligand escape from myoglobin proteins at room temperature. *J. Am. Chem. Soc.* 112:4680–4687.
- Chothia, C. 1975. Structural invariants in protein folding. *Nature*. 254: 304–308.
- Chu, K., J. Vojtechovsky, B. H. McMahon, R. M. Sweet, J. Berendzen, and I. Schlichting. 2000. Structure of a ligand-binding intermediate in wild-type carbonmonoxy myoglobin. *Nature*. 403:921–923.
- Egeberg, K. D., B. A. Springer, S. G. Sligar, T. E. Carver, R. J. Rohlfis, and J. S. Olson. 1990. The role of Val68(E11) in ligand binding to sperm whale myoglobin. Site-directed mutagenesis of a synthetic gene. *J. Biol. Chem.* 265:11788–11795.
- Elber, R., and M. Karplus. 1990. Enhanced sampling in molecular dynamics: use of the time-dependence Hartree approximation for a simulation of carbon monoxide diffusion through myoglobin. *J. Am. Chem. Soc.* 112:9161–9175.
- Gibson, Q. H., R. Regan, R. Elber, J. S. Olson, and T. E. Carver. 1992. Distal pocket residues affect picosecond ligand recombination in myoglobin. *J. Biol. Chem.* 267:22022–22034.
- Hartmann, H., S. Zinser, P. Komninos, R. T. Schneider, G. U. Nienhaus, and F. Parak. 1996. X-ray structure determination of a metastable state of carbonmonoxy myoglobin after photodissociation. *Proc. Natl. Acad. Sci. U.S.A.* 93:7013–7016.
- Henry, E. R., J. H. Sommer, J. Hofrichter, and W. A. Eaton. 1983. Geminate recombination of carbon monoxide to myoglobin. *J. Mol. Biol.* 166:443–451.
- Huang, X., and S. G. Boxer. 1994. Discovery of new ligand binding pathways in myoglobin by random mutagenesis. *Nat. Struct. Biol.* 1:226–229.
- Hubbard, S. R., W. A. Hendrickson, D. G. Lambright, and S. G. Boxer. 1990. X-ray crystal structure of a recombinant human myoglobin mutant at 2.8 Å resolution. *J. Mol. Biol.* 213:215–218.
- Ikeda-Saito, M., Y. Dou, T. Yonetani, J. S. Olson, T. Li, R. Regan, and Q. H. Gibson. 1993. Ligand diffusion in the distal heme pocket of myoglobin. *J. Biol. Chem.* 268:6855–6857.
- Krzywda, S., G. N. Murshudov, A. M. Brzozowski, M. Jaskolski, E. E. Scott, S. A. Klizas, Q. H. Gibson, J. S. Olson, and A. J. Wilkinson. 1998. Stabilizing bound O $_2$ in myoglobin by valine⁶⁸(E11) to asparagine substitution. *Biochemistry*. 37:15896–15907.
- Kunkel, T. A. 1985. Rapid and efficient site-specific mutagenesis without phenotypic selection. *Proc. Natl. Acad. Sci. U.S.A.* 82:488–492.
- Laird, B. B., and J. L. Skinner. 1989. Microscopic theory of reversible pressure broadening in hole-burning spectra of impurities in glasses. *J. Chem. Phys.* 90:3274–3281.
- Lambright, D. G., S. Balasubramanian, and S. G. Boxer. 1989. Ligand and proton exchange dynamics in recombinant human myoglobin mutants. *J. Mol. Biol.* 207:289–299.
- Li, T., M. L. Quillin, G. N. Phillips, Jr., and J. S. Olson. 1994. Structural determinants of the stretching frequency of CO bond to myoglobin. *Biochemistry*. 33:1433–1446.

- Lim, M., T. A. Jackson, and P. A. Anfinrud. 1997. Ultrafast rotation and trapping of carbon monoxide dissociated from myoglobin. *Nat. Struct. Biol.* 4:209–214.
- Ma, J., S. Huo, and J. E. Straub. 1997. Molecular dynamics simulation study of the B-states of solvated carbon monoxymyoglobin. *J. Am. Chem. Soc.* 119:2541–2551.
- Meller, J., and R. Elber. 1998. Computer simulations of carbon monoxide photodissociation in myoglobin: structural interpretation of the B states. *Biophys. J.* 74:789–802.
- Morikis, D., P. M. Champion, B. A. Springer, and S. G. Sligar. 1989. Resonance Raman investigations of site-directed mutants of myoglobin: effects of distal histidine replacement. *Biochemistry*. 28:4791–800.
- Oldfield, E., K. Guo, J. D. Augspurger, and C. E. Dykstra. 1991. A molecular model for the major conformational substrates in heme proteins. *J. Am. Chem. Soc.* 113:7537–7541.
- Olson, J. S., and G. N. Phillips, Jr. 1996. Kinetic pathways and barriers for ligand binding to myoglobin. *J. Biol. Chem.* 271:17593–17596.
- Ostermann, A., R. Waschipky, F. G. Parak, and G. U. Nienhaus. 2000. Ligand binding and conformational motions in myoglobin. *Nature*. 404:205–208.
- Phillips, G. N., Jr., M. L. Teodoro, T. Li, B. Smith, and J. S. Olson. 1999. Bound CO is a molecular probe of electrostatic potential in the distal pocket of myoglobin. *J. Phys. Chem. B*. 103:8817–8829.
- Quillin, M. L., T. Li, J. S. Olson, G. N. Phillips, Jr., Y. Dou, M. Ikeda-Saito, R. Regan, M. Carlson, Q. H. Gibson, H. Li, and R. Elber. 1995. Structural and functional effects of apolar mutations of the distal valin in myoglobin. *J. Mol. Biol.* 245:416–436.
- Rohlfs, R. J., A. J. Mathews, T. E. Carver, J. S. Olson, B. A. Springer, K. D. Egeberg, and S. G. Sliger. 1990. The effects of amino acid substitution at position E7 (residue 64) on the kinetics of ligand binding to sperm whale myoglobin. *J. Biol. Chem.* 265:3168–3176.
- Schlichting, I., J. Berendzen, G. N. Phillips, Jr., and R. M. Sweet. 1994. Crystal structure of photolysed carbonmonoxy-myoglobin. *Nature*. 371:808–812.
- Scott, E. E., and Q. H. Gibson. 1997. Ligand migration in sperm whale myoglobin. *Biochemistry*. 36:11909–11917.
- Smerdon, S. J., G. G. Dobson, A. J. Wilkinson, Q. H. Gibson, R. S. Blackmore, T. E. Carver, and J. S. Olson. 1991. Distal pocket polarity in ligand binding to myoglobin: structural and functional characterization of a threonine⁶⁸(E11) mutant. *Biochemistry*. 30:6252–6260.
- Srajer, V., T. Teng, T. Ursby, C. Pradervand, Z. Ren, S. Adachi, W. Schildkamp, D. Bourgeois, M. Wulff, and K. Moffat. 1996. Photolysis of the carbon monoxide complex of myoglobin: nanosecond time-resolved crystallography. *Science*. 274:1726–1729.
- Uchida, T., K. Ishimori, and I. Morishima. 1997. The effects of heme pocket hydrophobicity on the ligand binding dynamics in myoglobin as studied with leucine 29 mutants. *J. Biol. Chem.* 272:30108–30114.
- Varadarajan, R., D. G. Lambright, and S. G. Boxer. 1989. Electrostatic interactions in wild-type and mutant recombinant human myoglobins. *Biochemistry*. 28:3771–3781.
- Varadarajan, R., A. Szabo, and S. G. Boxer. 1985. Cloning, expression in *Escherichia coli*, and reconstitution of human myoglobin. *Proc. Natl. Acad. Sci. U.S.A.* 82:5681–5684.
- Vojtechovsky, J., K. Chu, J. Berendzen, R. M. Sweet, and I. Schlichting. 1999. Crystal structures of myoglobin-ligand complexes at near-atomic resolution. *Biophys. J.* 77:2153–2174.